# ROLE OF CARBONIC ANHYDRASES IN SKIN WOUND HEALING

Marleena Aaltonen
Syventävien opintojen kirjallinen työ
Tampereen Yliopisto
Lääketieteen ja Biotieteiden tiedekunta
Professori Tero Järvisen tutkimusryhmä
Toukokuu 2016

Tampereen yliopisto
Lääketieteen ja Biotieteiden tiedekunta
Professori Tero Järvisen tutkimusryhmä

AALTONEN MARLEENA: ROLE OF CARBONIC ANHYDRASES IN SKIN WOUND HEALING

Kirjallinen työ, 35 s.
Ohjaaja: professori Tero Järvinen

Toukokuu 2016

Avainsanat: CA IV, CA IX, re-epithelialization, angiogenesis, cell migration

Ihohaavan paraneminen alkaa re-epitelisaatiolla keratinosyyttien vaeltaessa haavan reunoilta kohti toisiaan. Solumigraatio alkaa jo ennen verisuonten uudismuodostusta, jolloin haavassa vallitsee hypoksiset olosuhteet. Syöpäsoluja tutkittaessa on havaittu, että hypoksia ja hapan ympäristö stimuloivat solumigraatiota. Hiilihappoanhydraasit (CA) ovat entsyymejä, jotka osallistuvat happo-emästasapainon säätelyyn katalysoimalla hiilidioksidin reversiibeliä hydrataatiota bikarbonaatti-ioniksi ja protoniksi.

Tutkimuksessa selvitimme hiilihappoanhydraasien roolia ihohaavan paranemisessa. Havaitsimme, että CA IX sekä erityisesti CA IV ekspressoituivat ihohaavassa voimakkaasti 2-5 vuorokauden kohdalla, mikä antoi vahvoja viitteitä ko. entsyymien osallisuudesta haavan luonnolliseen paranemisprosessiin hypoksisen vaiheen aikana. Jatkotutkimuksessa selvitimme nopeuttaako CA IV ihohaavan paranemista hiirillä ja toisaalta hidastaako endogeenisen CA IV:n eliminointi sitä. Tutkittavia aineita lisättiin suoraan haavoihin ja haavat kerättiin viiden vuorokauden kuluttua. Paranemista arvioitiin määrittämällä histologisista näytteistä re-epitelisaation ja granulaatiokudosmuodostuksen aste sekä makroskooppisesti haavan koon perusteella.

Re-epitelisaatiossa havaittiin tilastollisesti merkitsevä ero ryhmien välillä: CA IV:llä hoidetuilla hiirillä ihohaava sulkeutui nopeammin sekä inhibiittori- että kontrolliryhmään nähden. Sen sijaan inhibiittoriryhmässä oletettua haavan paranemisen hidastumista ei havaittu.

**CONTENT**

# ROLE OF CARBONIC ANHYDRASES IN SKIN WOUND HEALING

Harlan Barker[1#], Marleena Aaltonen[1#], Peiwen Pan[1], Maria Vähätupa[1], Pirkka Kaipiainen[1], Ulrike May[1], Stuart Prince[1], Hannele Uusitalo-Järvinen[1,2], Abdul Waheed[3], Silvia Pastoreková[4], William S. Sly[3], Seppo Parkkila[1,2] & Tero A.H. Järvinen[1,2]

[1]School of Medicine, University of Tampere, Tampere, Finland

[2]Eye Centre, Fimlab laboratories & Department of Orthopedics & Traumatology, Tampere University Hospital, Tampere, Finland

[2]Edward A. Doisy Department of Biochemistry and Molecular Biology, Saint Louis University School of Medicine, Saint Louis, Missouri, USA

[3]Centre of Molecular Medicine, Institute of Virology, Slovak Academy of Sciences, Bratislava, Slovak Republic

[#]equally contributed

*Address for correspondence:

Prof. Tero Järvinen, M.D., Ph.D.

School of Medicine, FI-33014 University of Tampere, Finland

Phone: + 358-44-285 4620

Email: blteja@uta.fi

**Short title:** Carbonic anhydrases in skin wound.

# 1. ABSTRACT

Skin wound closure occurs when keratinocytes migrate from the edge of the wound and re-epithelialize the epidermis. Their migration takes place primarily before any vascularization is established, i.e. under hypoxia, but relatively little is known about the factors that stimulate it. Hypoxia and acidic environment are well-established stimuli for cancer cell migration. The carbonic anhydrases (CAs) contribute to tumor cell migration by generating acidic environment through conversion of carbon dioxide to bicarbonate and a proton. We explored the possible role of CAs in wound healing using mouse models of skin wound healing. We show that the expression of CA IV and IX mRNAs are increased during the wound hypoxic period (days 2-5) and the cells expressing CAs form a band-like structure underneath migrating epidermis. RNA Seq analysis suggested that the CA IV-specific signal in the wound is mainly derived from neutrophils. Due to the high induction of CA IV, we treated skin wounds locally with recombinant human CA IV enzyme. Recombinant CA IV accelerated wound re-epithelialization during the hypoxic phase. Thus, CA IV could contribute to wound healing by providing acidic environment for the migrating epidermis and may offer novel opportunities to accelerate wound healing in compromised conditions.

# 2. INTRODUCTION

The healing of a human skin wound is a complex and highly coordinated biological process involving diverse phenomena, such as hemostasis, inflammation, re-epithelialization, angiogenesis, fibroplasia, and finally tissue remodelling (Martin and Nunan, 2015; Woodley et al., 2015). "Re-epithelialization" is the lateral migration of keratinocytes across the wound bed which, when successful, closes the wound (Martin and Nunan, 2015; Woodley et al., 2015).

Re-epithelialization begins within hours after injury. It is believed that a critical switch for the initiation of cell migration by keratinocytes is the acute change in oxygen tension (Woodley et al., 2015). That is, when the skin is wounded and the dermal blood vessels are clotted and no longer able to deliver oxygen to the skin, the keratinocytes experience the stress of acute hypoxia, and start migration to close the defect. Remarkably, the re-epithelialization takes place mainly in hypoxia and the wound closure can be completed before any new re-vascularization takes place (Woodley et al., 2015).

Studies have shown that in addition to hypoxia, acidosis stimulates cancer cell migration (Benej et al., 2014; Pastorekova et al., 1997). Carbonic anhydrases (CA) are a family of zinc metalloenzymes that regulate the tissue acid-base equilibrium by catalysing the reversible hydration of carbon dioxide to bicarbonate ions and protons ($CO_2 + H_2O <-> HCO_3^- + H^+$) (Benej et al., 2014; Pastorekova et al., 1997; Waheed and Sly, 2014). 15 human CA isoforms have been found of which 12 are active and 3 inactive (Aspatwar et al., 2013; Hilvo et al., 2008). These isoenzymes are expressed to some extent in all tissues and organs, but particularly in those that are metabolically highly active such as the brain and kidney (Benej et al., 2014; Waheed and Sly, 2014). Interestingly, expression of CAs IX and XII are induced by hypoxia in different tumors (Ivanov et al., 2001). Through their ability to regulate pH and generate acidic environment, these enzymes endow tumor cells with survival advantages in hypoxia/acidosis and confer an increased ability to migrate.

The potency of CAs IX and XII to stimulate cell migration under hypoxia, prompted us to investigate the role of CAs in the skin wound healing. Quite unexpectedly, nothing is known about CAs during skin wound healing. We assumed that the expression of certain CA family members could increase when a wound is exposed to hypoxia and theoretically they could stimulate re-epithelialization by generating acidic environment for keratinocytes. Thus, we studied the

expression pattern of the enzymatically active CAs in wounds of mice, and based on those results also treated the wounds with exogenously added CA IV recombinant enzyme.

# 3. RESULTS

## 3.1 The expression of CA IV and CA IX are induced during the hypoxic phase of wound healing

To investigate the role of CAs in the skin wound healing process, we determined the expression pattern of 11 active members of the CA family (CA I, II, III, IV, Vb, VI, VII, IX, XII, XIII and XV) by qPCR analysis of wounds at different stages of healing , and compared their expression to the levels seen in normal, unwounded skin. Hypoxia persists in our excision wound model for five days after wounding, after which extensive angiogenesis vascularizes the wound bed and the wound is supplied with oxygen (Järvinen and Ruoslahti, 2007). Among the CA family members, the expression of CA IV mRNA was induced most strongly at almost 25-fold above normal two days after the wounding and remained elevated to more than 5-fold at five days after the wounding (Figure 1). CA IX was the only other enzyme that showed elevated expression during wound healing; its expression peaked at three days to a level more than 4-fold that of normal skin and the expression remained elevated at day 5 of the healing (Figure 1). After the skin wound is vascularized (from day 5 on), none of the CAs showed any enhanced expression at the mRNA level (Figure 1).

As CAs IV and IX showed increased mRNA expression during the hypoxic phase of the wound healing, we decided to explore their expression in greater detail by immunohistochemistry. CA IV protein expression started to accumulate in the early granulation tissue at day 5 of the healing and positive expression remained in the wound until day 10, after which the expression disappeared (Figure 2). CA IV protein was expressed mainly by the cells in granulation tissue with especially strong, band-like, expression just beneath migrating epidermis (Figure 2). CA IX protein expression, in turn, was already seen in the skin wound at day 2 and remained elevated throughout the wound healing process, i.e. after CA IV had disappeared from the wound tissue (Figure 2). Both the epidermis and underlying granulation tissue expressed CA IX, but the strongest CA IX protein

expression was also seen in the migrating epidermis and just beneath the migrating epidermis in the top layer of dermis (Figure 2).

## 3.2 CA transcripts in wound-related cells

To elucidate the cell sources that produce CAs during wound healing, a thorough analysis of human RNA-Seq data was performed. RNA-Seq analysis of 12 cell types revealed that a CA4 transcript is expressed significantly only in skin and neutrophils (Figure 3). In both tissues only the 312 amino acid ENST00000300900 CA4 transcript is expressed. In the skin a total of 12 CA genes are expressed (Supplementary Table 2). Of these, CA4 has one of the lowest levels of expression with a normalized FPKM value of 160.18. In neutrophils the CA4 expression level is significantly higher than in skin with a FPKM of 7162.48. CA9 expression was significant in fibroblasts, skin, and macrophages (Figure 3), with expression in fibroblasts significantly higher than the others.

## 3.3 Characterization of CA4 promoter

The unexpected and high level induction of CA4 mRNA in the skin wound prompted us to characterize the CA4 promoter in detail to provide clues on the potential regulation of its transcription. Our comparative genomics analysis of the aligned CA4 promoter regions of 15 mammal species revealed a distinct cluster of high scoring and well conserved potential transcription factor binding sites immediately upstream of a similarly predicted TATA-binding protein binding site (Figure 4). Present in all 15 species is a strong signal for a CTCF binding site located from -55 to -44 bp upstream of the TSS (Figure 4). In 13 of the species, including human, this region is an exact match for previously experimentally determined CTCF binding sites. Overlapping the probable CTCF site are predicted binding sites for SP1, KLF4, and MZF1. The SP1 and MZF1 sites are a match for previously experimentally determined sites in all 15 species, while the KLF4 is a match in 14 species. The locations of binding are: -55 to -44 on the sense-strand (CTCF), -50 to -39 on the anti-sense strand (SP1), -47 to -41 on the sense-strand (MZF1), and -49 to -39 on the sense-strand (KLF4) (Figure 4). Importantly, our results did not reveal any HIF-1αbinding sites in the CA4 promoter.

## 3.4 GO analysis of biological processes associated with CA4 in skin

Next we wanted to understand the potential function of CA4 in skin wound healing and thus, performed gene ontology enrichment (GO) analysis of biological processed associated with CA4 expression. GO enrichment analysis of genes with a strong expression correlation (≥0.50) with CA4 in skin resulted in a total of 40 terms which were represented two-fold or higher in our set versus what was expected (Supplementary Table 3). The terms which had the highest over-representation in our set were strongly related to immune cell recruitment. Additionally, terms related to angiogenesis, endocytosis, inflammation, and ion homeostasis were also over-represented.

## 3.5 Expression of Car4 is not induced by hypoxia in pure hypoxia-driven angiogenesis-model

To explore whether hypoxia induced the expression of Car4 during wound healing, we next employed a pure hypoxia-driven angiogenesis of oxygen-induced retinopathy model (OIR). We could not detect any induction of Car4 mRNA either by the hypoxia at P12 or by revascularization at P17 ruling out the possibility that CA4 is a hypoxia inducible gene (Supplementary Figure 1).

## 3.6 Expression and characterization of recombinant CA IV

To further explore the function of CA IV in skin wound healing, we produced and purified recombinant CA IV enzyme. CA IV is especially suitable for therapeutic applications as it is an extracellular enzyme and has one of the highest enzymatic activity levels of the CAs. In SDS gel electrophoresis, a major band was identified at 30 kDa representing a full length recombinant CA IV (Supplementary Figure 2). The affinity purified CA IV enzyme had a specific activity of 3000 - 4000 unit/mg of pure enzyme.

## 3.7 Wound treatment with CA IV and acetazolamide

Next, we examined the effects of recombinant CA IV and endogenously expressed CAs on wound healing, focusing on the re-epithelialization obtained by keratinocyte migration. Rodents can close wounds by two different means: wound contraction or by true re-epithelialization (Davidson et al., 2013). To alleviate wound contraction and to explore re-epithelialization specifically, a special skin excision wound-model was employed, where a round silicone splint is sutured into the skin to

firmly attach the underlying dermis and subcutis (Davidson et al., 2013). The wounded animals were divided into three groups that received topically applied saline (control), recombinant CA IV enzyme, or CA inhibitor (azetazolamide) in Pluronic-127 gels (Blanc-Brude et al., 2002). No differences were detected in the size of wounds immediately after wounding or at the size of the scab covering the wound at the end of treatment trial (Supplementary Figure 3). The recombinant CA IV enhanced the wound re-epithelialization (Figure 5). The epithelial tongues were significantly longer in the recombinant CA IV-treated wounds than in the control wounds ($P<0.0001$) (Figure 5). We could not see any difference in the amount of granulation tissue produced in the wounds between the three treatment groups (Figure 5).

# 4. Discussion

Skin wound closure is obtained by re-epithelialization, i.e. lateral migration of the keratinocytes. It occurs mainly under hypoxia, but the stimuli for it are poorly understood. The present study shows that mRNA expression of two members of the CA family, CA IV and IX, are increased during the early phase of wound healing, and the cells expressing the CAs form a band-like structure just underneath the migrating epidermis in the healing skin wound. Furthermore, we demonstrate that exogenously added recombinant Car4 enzyme accelerates wound re-epithelialization during the hypoxic phase of wound healing.

In hypoxic tissues, such as fast growing cancers and wounds, metabolic processes produce high amounts of both lactic acid and carbon dioxide. CAs are enzymes that convert carbon dioxide and water to bicarbonate and protons (Benej et al., 2014; Pastorekova et al., 1997; Waheed and Sly, 2014). Because the intracellular pH has to remain stable, all excess acidity is efficiently exported from the cells. This, in turn, makes the extracellular environment acidic which provides a favorable environment for cancer cell migration and invasion (Pastorekova et al., 2006). CAs have been linked to this process by reports showing that the cancer cell invasion can be reduced by CA inhibitors whereas the expression of CAs, in turn, facilitates the cancer cell migration and invasion (Pastorekova et al., 2006).

Of the two CAs that showed enhanced expression during wound healing, CA IX is known to be induced by hypoxia. It has a hypoxia-response element (HRE) in its promotor region and is one of the known target genes for hypoxia inducible factor-1α (HIF-1α) (Benej et al., 2014; Pastorekova et al., 1997). Strikingly, the expression of CA IV was substantially higher than CA IX at mRNA level during hypoxia in the skin wound. The expression of CA IV is usually reduced in tumors (Niemela et al., 2007), and the present results show that it does not possess a classical HRE in its promoter region where HIF-1α could bind. Furthermore, we employed a pure hypoxia driven angiogenesis model in retina and could not detect any changes in the expression of Car4 by varying oxygen levels. Our results, in essence, rule out the possibility that hypoxia is responsible for the induction of Car4 expression.

The comparative genomics prediction of potential transcription factor binding sites in the promoter of primary human CA4 transcript ENST00000300900 revealed some high-scoring candidates that may alter the expression of this protein. In particular, there is a cluster of well conserved binding sites for KLF4, SP1, and MZF1 which were all near a similarly conserved CTCF binding site. CTCF is a well-established actor in chromatin configuration and gene transcription across the genome (Vietri Rudan and Hadjur, 2015), as such its presence and proximity gives greater weight to the other proximal predictions. MZF1 is involved in myeloid cell differentiation (Hui et al., 1995), thus potentially explaining the origin of strong CA4 expression in neutrophils. KLF4, in turn, has been shown to be expressed in inflammation (Sevilla et al., 2015) and wound healing (Kaushik et al., 2010; Li et al., 2012; Liu et al., 2015; Ou et al., 2015).

Our RNA-Seq analysis showed low levels of CA4 RNA in normal skin and high levels in neutrophils. This implies that the observed elevation of CA4 mRNA and protein in our experiments may be due to recruitment of neutrophils to the wound site, which is in line with the fact that abundant neutrophil extravasation takes place in skin wounds rapidly after wounding. Interestingly, those few neutrophils that persist in the wound are known to make a band-like formation just underneath the migrating epidermis (Grguric-Smith et al., 2015). Especially strong production of CA IV and IX just beneath the migrating epidermis suggests that these enzymes could generate an acidic “micro-environment” within healing wound tissue to aid selectively the keratinocyte migration, i.e. closure of the wound.

Concerning CA IX expression in skin wound, RNA-Seq analysis confirmed expression of CA9 mRNA in only fibroblasts and skin, with that in fibroblasts being significantly higher. The CA IX protein has been shown to be upregulated in tumor fibroblasts undergoing hypoxia (Ishii et al.,

2005; Santi et al., 2013); while fibroblast-derived HIF-1α has been shown to be crucial for wound healing (Duscher et al., 2015).

Based on the expression pattern of CA family members, we conclude that it is CAs IV and IX which are responsible for maintaining the pH-balance during the skin wound healing. We were able to see induction of CA IV and CA IX mRNAs during the early, hypoxic phases of the wound healing and both mRNAs returned to the same level as normal skin in seven days. This implies that there is rapid induction of these proteins in response to hypoxia (HIF1α-mediated for CA IX) and inflammation (CA IV).

To understand the function of CAs in tissue regeneration in general, we treated skin wounds with recombinant human CA IV enzyme and also with a clinically used CAs inhibitor to block the endogenously expressed CA activity. We could detect accelerated wound re-epithelialization by recombinant CA IV, but the blocking of endogenously expressed CA activity showed no significant effect on the wound re-epithelialization. This discrepancy is explained most likely by the fact that endogenous CA-accumulation in the skin wound starts at least a few days after the wounding. Thus, the CA inhibitor was unlikely to encounter any enhanced CA protein expression during the majority of our study period (Days 0 – 5), whereas the exogenously added recombinant CA enzyme provided a clear benefit over endogenous enzyme as it was present in the wound immediately after the wounding. This is highly relevant for CA4 as our data indicates that its primary source in the wound bed is neutrophils, which start to extravasate to the wound within several hours after the injury.

Future studies are warranted to address whether CAs could be used to stimulate tissue regeneration during injury induced hypoxia. CA IV may participate in promoting tissue regeneration by generating an acidic “micro-environment” for migrating epidermis to close the wound during hypoxic phase of wound healing.

# 5. MATERIALS AND METHODS

## 5.1 Generation of skin wounds

For the qPCR and immunohistochemistry analyses, eight-week-old male BALB/c mice (weighing 23–25 g) were used. Mice were fed with standard laboratory pellets and water *ad libitum*. All

animal experiments were performed in accordance with protocols approved by the National Animal Ethics Committee of Finland.

6-mm diameter, full thickness (including *panniculus carnosus* muscle) excision wounds were made in the dorsal skin under sevoflurane-anesthesia as described previously (Järvinen and Ruoslahti, 2007). At various time-points the animals were sacrificed and the wounded tissue collected and processed for further analyses.

## 5.2 Quantitative PCR (qPCR) analysis

Total skin wound RNA from various time-points was converted to cDNA by reverse transcription using the High capacity cDNA reverse transcription Kit for RT-qPCR (Applied Biosytems Inc, CA, USA). Duplicate qRT-PCR reactions were performed with PowerSYBR SybrGreen reagents (Applied Biosytems Inc, CA, USA) on an ABI 7000 Real Time PCR System (Applied Biosytems Inc, CA, USA). Details for primers used are listed in Supplementary Table 1. As negative controls, no-template and no-reverse transcriptase controls were also included (which were herein negative). Data analyses were performed according to Livak and Schmittgen (Livak and Schmittgen, 2001).

## 5.3 Expression and purification of recombinant human CA IV

cDNA for the secretory form of human CA IV was cloned in pET-11d, a bacterial expression vector, as described previously (Waheed et al., 1997). Briefly, the E. coli strain Rosetta(DE3)pLysS was used for enzyme production. The enzyme was purified using a CA-inhibitor affinity column (Waheed et al., 1997). Affinity pure enzyme was dialyzed against 20 mM ammonium bicarbonate for several changes of the buffer. Endotoxin removal was performed by using a specialized endotoxin removal column three times (Hyglos Blue Endotoxin Removal Column, Starnberg, Germany). The protein samples were then re-dialyzed with saline, filter-sterilized, and stored at 4 °C. Recombinant CA IV was analyzed on an Invitrogen NuPAGE 4–12% gradient gel (Life Technologies). The enzymatic activity of recombinant CA IV was assayed as described previously (Waheed et al., 1997).

## 5.4 Skin wound treatment trial with recombinant CA IV

For the treatment trial, male littermate BALB/c mice of age 8 weeks were used. Two 6 mm circular, full thickness wounds were generated in each animal by biopsy punch. A donut-shaped 12-mm silicone splint (Grace Bio-Labs) was placed around the wounds and affixed with glue and sutures in order to prevent wound contraction (Davidson et al., 2013). Mice were given plastic collars to prevent them from tearing off the splints (Davidson et al., 2013). The operated mice were divided to three groups. The first group consisted of mice treated with CA IV; purified CA IV was mixed in 30 % Pluronic-127 (Sigma-Aldrich) gel as described previously (Blanc-Brude et al., 2002). 50 µl of the mixture was added to each wound to fill up the entire wound cavity. The second group received a CA inhibitor, acetazolamide (1.0 mM, Orion, Espoo, Finland) in Pluronic-127 gel. The third group was used as a control group and was treated with 50 µl of PBS mixed with Pluronic-127 gel. The final concentration of Pluronic-127 in each solution was 18 %. Each mouse was photographed after the silicone splints had been sutured securely in place and then at sacrifice on day 5.

## 5.5 RNA-Seq analysis of wound-specific tissues

RNA-Seq data from human B-cells, CD4-positive cells, CD8-positive cells, monocytes, neutrophils, natural killer (NK) cells, monocytes (ArrayExpress accession E-GEOD-60424)(Linsley et al., 2014), dermal fibroblasts (E-GEOD-72589), undifferentiated and differentiated keratinocytes (E-MTAB-1717) (Jones et al., 2014), M1 and M2 macrophages (E-GEOD-36952), and skin cells (E-MTAB-2836) (Uhlen et al., 2015) were retrieved from the Array Express database. Reads for all samples were pooled by tissue type and mapped to *CA* genes in the human genome using the Bowtie (Langmead et al., 2009) and Tophat (Trapnell et al., 2009) modules of the Tophat package utilizing supercomputer resources provided by CSC – IT Center for Science of the Finnish Ministry of Education and Culture. Subsequent matches were then compared to reference CA transcript structures from the Ensembl database using the Cuffcompare module of the Cufflinks package (Trapnell et al., 2010). Normalized fragments per kilobase of transcript per million mapped reads (FPKM) values were generated for each transcript identified in each tissue using the Cuffnorm module of the Cufflinks package in order to compare expression values across pooled samples. A comparison of expression for each CA across tissue types was calculated using the Cuffmerge and Cuffdiff modules of Cufflinks. Results were visualized using the cummeRbund R library.

### 5.6 Statistical analysis

Data was presented as mean ± standard deviation. For comparisons of multiple groups, statistical analysis was carried out by two-way analysis of variance (ANOVA) complemented by the Bonferroni post hoc test for pair wise comparisons between the test groups. P-value < 0.05 was considered significant.

### 5.7 Supplementary Methods

Extraction of RNA, oxygen induced retinopathy (OIR) model, immunohistochemistry, histology, quantitative analysis of histology, promoter analysis of the primary CA4 transcript and GO analysis of proteins were performed using standard methods (Jarvinen and Ruoslahti, 2010; May et al., 2015; Mi et al., 2013; Uusitalo-Jarvinen et al., 2007) and are described in detail in Supplementary data set.

## 6. CONFLICT OF INTEREST

Authors report no conflict of interest.

## 7. ACKNOWLEDGEMENTS

We thank Marianne Karlsberg, and Marja-Leena Koskinen for practical support, histochemical work and for immunohistological stainings. The work was funded by the Sigrid Juselius Foundation, the Academy of Finland, Päivikki and Sakari Sohlberg Foundation, Instrumentarium Research Foundation, Finnish Medical Foundation, Pirkanmaa Hospital District Research Foundation and the Finnish Cultural Foundation. We also thank CSC – IT Center for Science of the

Finnish Ministry of Education and Culture for providing the high-performance computing resources needed to perform the computational analyses.

## 8. CONTRIBUTIONS

TJ, MA, HU-J and SPar designed the research. SPas raised the CA IX antibody. AW and WSS produced the recombinant CA IV enzyme and raised the CA IV antibody. HB performed comparative genomics, RNA-Seq, and GO enrichment computational analyses. MA, HB, PK, PP, MV, UM and SPar performed the research. MA, HB, PP, SPar and TJ analyzed the data. MA, HB, SPar, and TJ wrote the manuscript. MA, HB, PP, SPar and TJ made the figures. All authors reviewed and accepted the text of the manuscript.

## 9. ABBREVIATIONS

CA4 – Human carbonic anhydrase 9 gene; Car4 – Mouse carbonic anhydrase 9 gene; CA9 – Human carbonic anhydrase 9 gene; Car9 – Mouse carbonic anhydrase 9 gene; CA IV – Carbonic anhydrase 4 protein; CA IX – Carbonic anhydrase 9 protein

# 10. REFERENCES

(1) Woodley DT, Wysong A, DeClerck B, Chen M, Li W. Keratinocyte Migration and a Hypothetical New Role for Extracellular Heat Shock Protein 90 Alpha in Orchestrating Skin Wound Healing. Adv Wound Care (New Rochelle) 2015 Apr 1;4(4):203-212.

(2) Martin P, Nunan R. Cellular and molecular mechanisms of repair in acute and chronic wound healing. Br J Dermatol 2015 Aug;173(2):370-378.

(3) Benej M, Pastorekova S, Pastorek J. Carbonic anhydrase IX: regulation and role in cancer. Subcell Biochem 2014;75:199-219.

(4) Pastorekova S, Parkkila S, Parkkila AK, Opavsky R, Zelnik V, Saarnio J, et al. Carbonic anhydrase IX, MN/CA IX: analysis of stomach complementary DNA sequence and expression in human and rat alimentary tracts. Gastroenterology 1997 Feb;112(2):398-408.

(5) Waheed A, Sly WS. Membrane associated carbonic anhydrase IV (CA IV): a personal and historical perspective. Subcell Biochem 2014;75:157-179.

(6) Hilvo M, Innocenti A, Monti SM, De Simone G, Supuran CT, Parkkila S. Recent advances in research on the most novel carbonic anhydrases, CA XIII and XV. Curr Pharm Des 2008;14(7):672-678.

(7) Aspatwar A, Tolvanen ME, Parkkila S. An update on carbonic anhydrase-related proteins VIII, X and XI. J Enzyme Inhib Med Chem 2013 Dec;28(6):1129-1142.

(8) Ivanov S, Liao SY, Ivanova A, Danilkovitch-Miagkova A, Tarasova N, Weirich G, et al. Expression of hypoxia-inducible cell-surface transmembrane carbonic anhydrases in human cancer. Am J Pathol 2001 Mar;158(3):905-919.

(9) Järvinen TA, Ruoslahti E. Molecular changes in the vasculature of injured tissues. Am J Pathol 2007 Aug;171(2):702-711.

(10) Davidson JM, Yu F, Opalenik SR. Splinting Strategies to Overcome Confounding Wound Contraction in Experimental Animal Models. Adv Wound Care (New Rochelle) 2013 May;2(4):142-148.

(11) Blanc-Brude OP, Yu J, Simosa H, Conte MS, Sessa WC, Altieri DC. Inhibitor of apoptosis protein survivin regulates vascular injury. Nat Med 2002 Sep;8(9):987-994.

(12) Pastorekova S, Parkkila S, Zavada J. Tumor-associated carbonic anhydrases and their clinical significance. Adv Clin Chem 2006;42:167-216.

(13) Niemela AM, Hynninen P, Mecklin JP, Kuopio T, Kokko A, Aaltonen L, et al. Carbonic anhydrase IX is highly expressed in hereditary nonpolyposis colorectal cancer. Cancer Epidemiol Biomarkers Prev 2007 Sep;16(9):1760-1766.

(14) Vietri Rudan M, Hadjur S. Genetic Tailors: CTCF and Cohesin Shape the Genome During Evolution. Trends Genet 2015 Nov;31(11):651-660.

(15) Hui P, Guo X, Bradford PG. Isolation and functional characterization of the human gene encoding the myeloid zinc finger protein MZF-1. Biochemistry 1995 Dec 19;34(50):16493-16502.

(16) Sevilla LM, Latorre V, Carceller E, Boix J, Vodak D, Mills IG, et al. Glucocorticoid receptor and Klf4 co-regulate anti-inflammatory genes in keratinocytes. Mol Cell Endocrinol 2015 Sep 5;412:281-289.

(17) Kaushik DK, Gupta M, Das S, Basu A. Kruppel-like factor 4, a novel transcription factor regulates microglial activation and subsequent neuroinflammation. J Neuroinflammation 2010 Oct 15;7:68-2094-7-68.

(18) Liu J, Zhang C, Liu Z, Zhang J, Xiang Z, Sun T. Honokiol downregulates Kruppel-like factor 4 expression, attenuates inflammation, and reduces histopathology after spinal cord injury in rats. Spine (Phila Pa 1976) 2015 Mar 15;40(6):363-368.

(19) Ou L, Shi Y, Dong W, Liu C, Schmidt TJ, Nagarkatti P, et al. Kruppel-like factor KLF4 facilitates cutaneous wound healing by promoting fibrocyte generation from myeloid-derived suppressor cells. J Invest Dermatol 2015 May;135(5):1425-1434.

(20) Li J, Zheng H, Wang J, Yu F, Morris RJ, Wang TC, et al. Expression of Kruppel-like factor KLF4 in mouse hair follicle stem cells contributes to cutaneous wound healing. PLoS One 2012;7(6):e39663.

(21) Grguric-Smith LM, Lee HH, Gandhi JA, Brennan MB, DeLeon-Rodriguez CM, Coelho C, et al. Neutropenia exacerbates infection by Acinetobacter baumannii clinical isolates in a murine wound model. Front Microbiol 2015 Oct 16;6:1134.

(22) Santi A, Caselli A, Paoli P, Corti D, Camici G, Pieraccini G, et al. The effects of CA IX catalysis products within tumor microenvironment. Cell Commun Signal 2013 Oct 29;11:81-811X-11-81.

(23) Ishii G, Sangai T, Ito T, Hasebe T, Endoh Y, Sasaki H, et al. In vivo and in vitro characterization of human fibroblasts recruited selectively into human cancer stroma. Int J Cancer 2005 Nov 1;117(2):212-220.

(24) Duscher D, Maan ZN, Whittam AJ, Sorkin M, Hu MS, Walmsley GG, et al. Fibroblast-Specific Deletion of Hypoxia Inducible Factor-1 Critically Impairs Murine Cutaneous Neovascularization and Wound Healing. Plast Reconstr Surg 2015 Nov;136(5):1004-1013.

(25) Livak KJ, Schmittgen TD. Analysis of relative gene expression data using real-time quantitative PCR and the 2(-Delta Delta C(T)) Method. Methods 2001 Dec;25(4):402-408.

(26) Waheed A, Pham T, Won M, Okuyama T, Sly WS. Human carbonic anhydrase IV: in vitro activation and purification of disulfide-bonded enzyme following expression in Escherichia coli. Protein Expr Purif 1997 Mar;9(2):279-287.

(27) Linsley PS, Speake C, Whalen E, Chaussabel D. Copy number loss of the interferon gene cluster in melanomas is linked to reduced T cell infiltrate and poor patient prognosis. PLoS One 2014 Oct 14;9(10):e109760.

(28) Jones M, Dry IR, Frampton D, Singh M, Kanda RK, Yee MB, et al. RNA-seq analysis of host and viral gene expression highlights interaction between varicella zoster virus and keratinocyte differentiation. PLoS Pathog 2014 Jan 30;10(1):e1003896.

(29) Uhlen M, Fagerberg L, Hallstrom BM, Lindskog C, Oksvold P, Mardinoglu A, et al. Proteomics. Tissue-based map of the human proteome. Science 2015 Jan 23;347(6220):1260419.

(30) Langmead B, Trapnell C, Pop M, Salzberg SL. Ultrafast and memory-efficient alignment of short DNA sequences to the human genome. Genome Biol 2009;10(3):R25-2009-10-3-r25. Epub 2009 Mar 4.

(31) Trapnell C, Pachter L, Salzberg SL. TopHat: discovering splice junctions with RNA-Seq. Bioinformatics 2009 May 1;25(9):1105-1111.

(32) Trapnell C, Williams BA, Pertea G, Mortazavi A, Kwan G, van Baren MJ, et al. Transcript assembly and quantification by RNA-Seq reveals unannotated transcripts and isoform switching during cell differentiation. Nat Biotechnol 2010 May;28(5):511-515.

(33) Jarvinen TA, Ruoslahti E. Target-seeking antifibrotic compound enhances wound healing and suppresses scar formation in mice. Proc Natl Acad Sci U S A 2010 Nov 24.

(34) May U, Prince S, Vähätupa M, Laitinen AM, Nieminen K, Uusitalo-Järvinen H, et al. Resistance of R-Ras knockout mice to skin tumour induction. Sci Rep 2015 Jul 2;5:11663.

(35) Uusitalo-Jarvinen H, Kurokawa T, Mueller BM, Andrade-Gordon P, Friedlander M, Ruf W. Role of protease activated receptor 1 and 2 signaling in hypoxia-induced angiogenesis. Arterioscler Thromb Vasc Biol 2007 Jun;27(6):1456-1462.

(36) Mi H, Muruganujan A, Casagrande JT, Thomas PD. Large-scale gene function analysis with the PANTHER classification system. Nat Protoc 2013 Aug;8(8):1551-1566.

# 11. FIGURE LEGENDS

## 11.1 Figure 1.

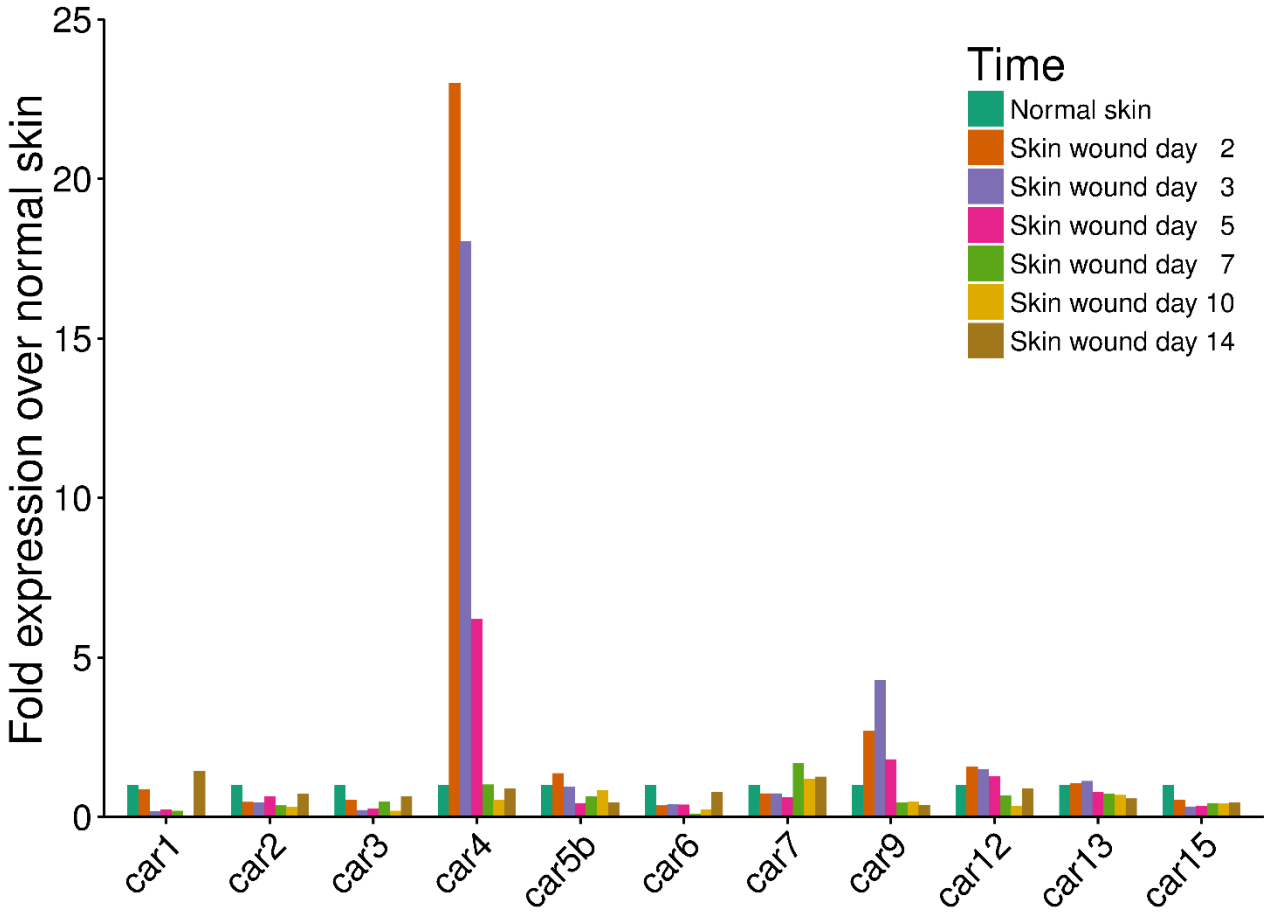


**Figure 1. mRNA expression of CA4 and CAIX during wound healing.**

Skin excision wounds were generated in WT mice as described in the methods. Normal skin and skin wound samples were collected from unwounded mice and from mice sacrificed at various time-points after wounding. The skin samples were processed for qPCR analysis as described in the methods. Results for all enzymatically active CAs are shown as mean ± SD. Animal numbers: unwounded: n = 2; Day 2: n = 2; Day 3: n = 2; Day 5: n = 3; Day 7: n = 2; Day 10: n = 2; Day 14: n = 2.

**11.2 Figure 2.**

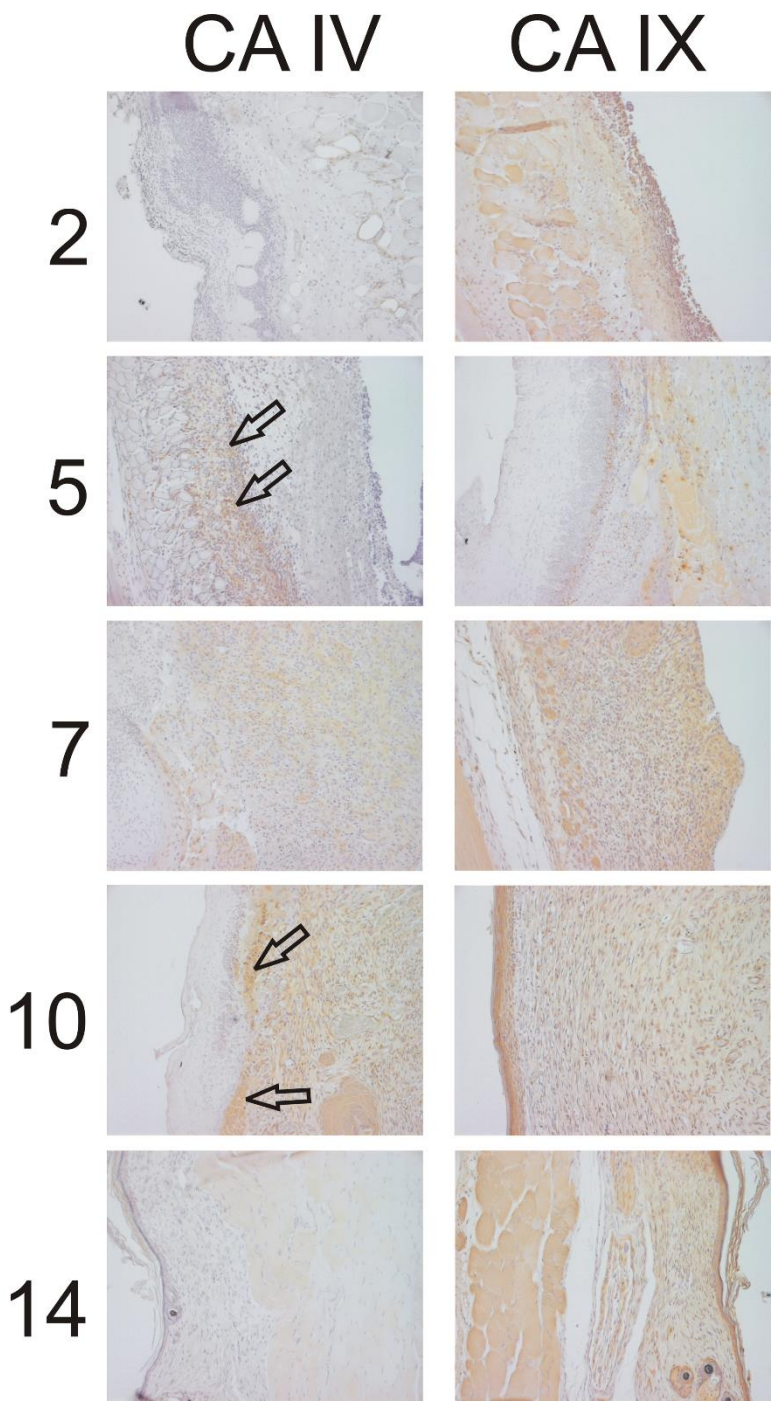


**Figure 2. Protein expression of Car4 and Car9 during wound healing.**

Skin excision wounds were generated in WT mice as described in the methods. Normal skin and skin wound samples were collected from unwounded mice and from mice sacrificed at various time-points after the wounding. The skin samples were processed for IHC analysis and CA IV and

CA IX were detected with specific antibodies as described in the supplementary methods. Results at all studied time-points are shown. CA IV protein expression started to accumulate in the early granulation tissue at day 5 of the healing and positive expression remained in the wound until day 10, after which the expression disappeared. CA IV protein was expressed mainly by the cells in granulation tissue with especially strong expression just beneath migrating epidermis. CA IX protein expression, in turn, was already seen in the skin wound at day 2 and remained elevated throughout the wound healing process. Animal numbers: All time-points n = 12.

## 11.3 Figure 3.

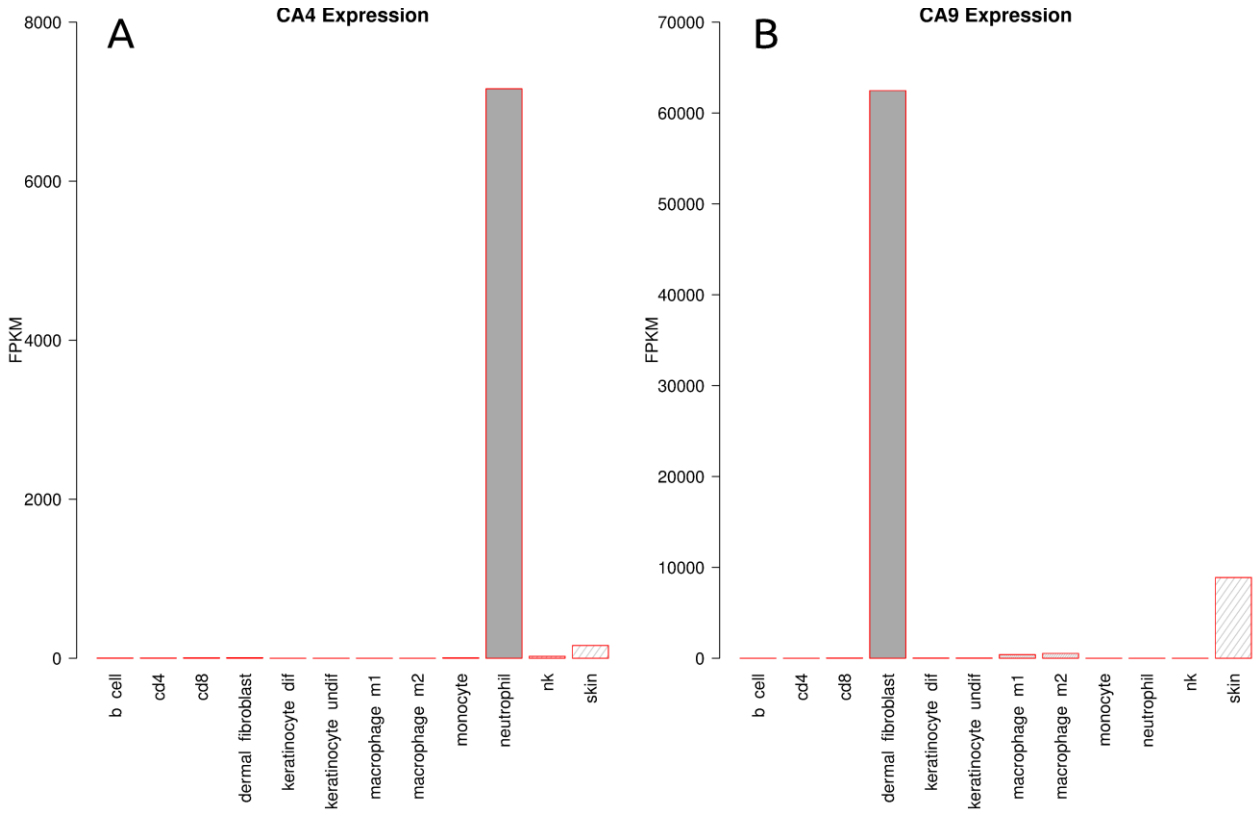


**Figure 3. Expression of CA4 and CA9 in wound related cells**

RNA-Seq data for multiple immune and wound healing related cells was retrieved from experiments housed in the ArrayExpress database and mapped to the genomic locations of all CA

genes using Tophat. The reads were then merged using Cuffmerge, and differential expression determined using Cuffdiff. Finally, the results were manipulated using the R package cummeRbund and visualized in R. Expression abundance measurements are represented on the y-axis as normalized fragments per kilobase of transcript per million mapped reads (FPKM) for CA4 (*A*) and CA9 (*B*).

## 11.4 Figure 4.

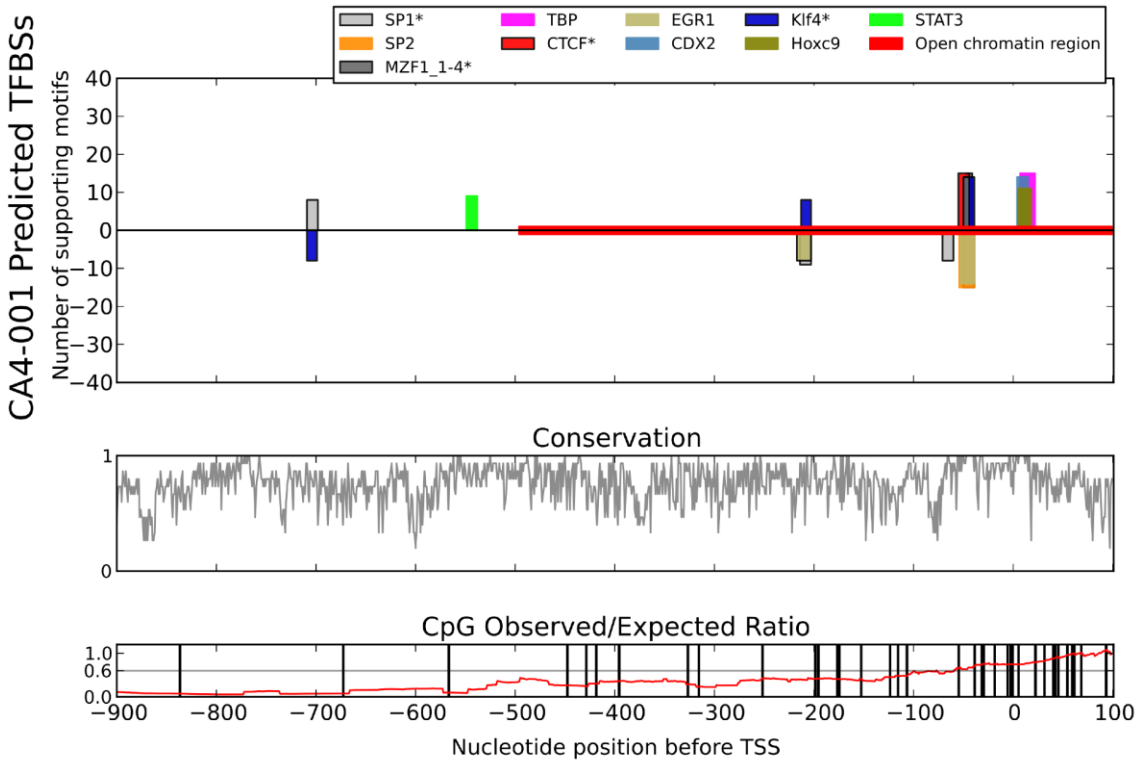


**Figure 4. Comparative genomics analysis of CA4 promoter.**

An alignment of 15 mammal sequences corresponding to the promoter of full length human CA4 transcript ENST00000300900 was analyzed for putative transcription factor binding sites by comparative genomics. The 10 best scoring transcription factors were included in the figure, where height indicates the number of species supporting that prediction. Positive y-axis results indicate a TFBS predicted on the sense strand while negative y-axis indicates the anti-sense strand.

## 11.5 Figure 5.

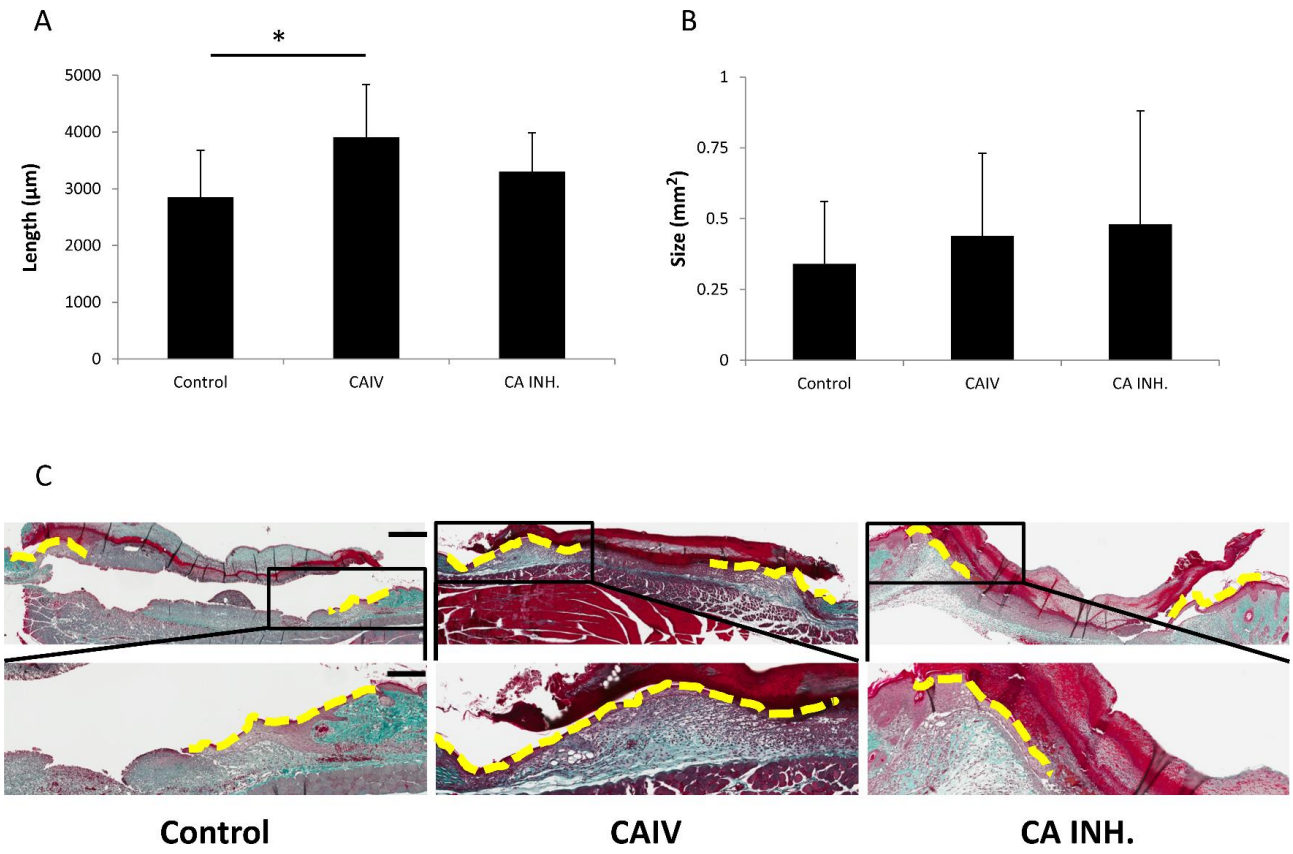


**Figure 5. Accelerated re-epithelialization during wound healing in mice treated with recombinant Car4 enzyme.**

Mice with full thickness skin excision wounds were treated with either recombinant Car4 enzyme or CA inhibitor applied on wound topically immediately after the wounding. Scars were harvested on day 5, and the re-epithelialization (*A*) and cross-sectional area of the granulation tissue (*B*) of the wounds were quantified by examining two microscopic sections from each wound. The results are expressed as the average of the two values. There were five animals, each with two wounds, in every treatment group. *$P < 0.05$; ANOVA. The results are expressed as mean ± SD, $n = 10$. (C) Representative sections from wounds treated with recombinant CAIV or CA inhibitor and collected

on day 5 after wounding are shown for re-epithelialization. Bars; 600 μm small magnification, 240 μm high magnification.

# 12. SUPPLEMENTARY INFORMATION

**Role of carbonic anhydrases in skin wound healing**

Harlan Barker, Marleena Aaltonen, Peiwen Pan, Maria Vähätupa, Ulrike May, Pirkka Kaipiainen, Stuart Prince, Hannele Uusitalo-Järvinen, Abdul Waheed, Silvia Pastoreková, William S. Sly, Seppo Parkkila & Tero A.H. Järvinen

# 13. SUPPLEMENTARY FIGURES

## 13.1 Supplementary Figure 1.

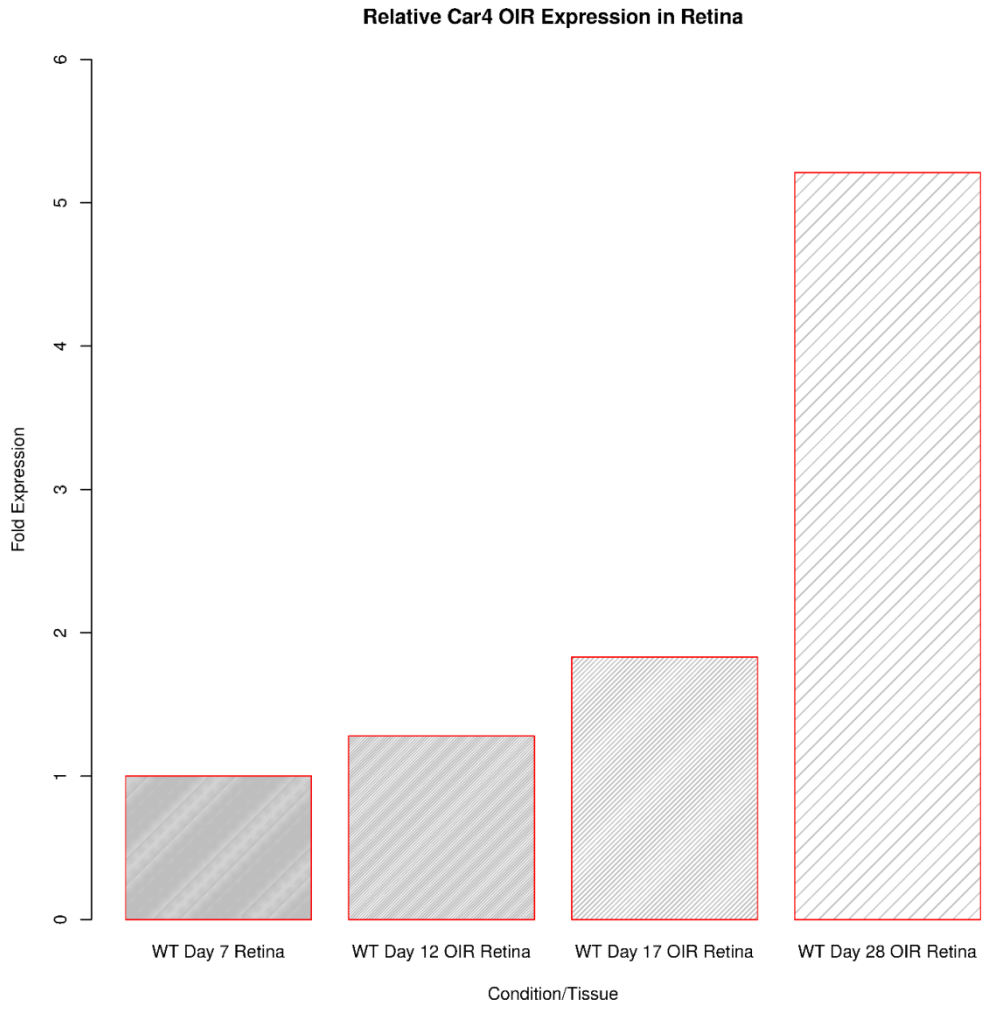


**Supplementary Figure 1. Expression of Car4 in oxygen induced retinopathy (OIR) model.**

The effects of hypoxia on Car4 mRNA expression in retina was studied with the OIR model. Retinas were harvested at P7, immediately after the exposure to hyperoxia (P12), after hypoxia-driven pathological angiogenesis has reached its maximum at P17 and when the retinal vasculature returns to normal at P28. Retinas were processed for qPCR analysis as described in methods. Results for Car4 are shown as mean ± SD. qPCR analysis of gene expression of the Car4 are shown

relative to the expression level in the normal retina at P7. Animal numbers: P7: n = 2; P12 OIR: n = 2; P17 OIR: n = 2; P28 OIR: n = 2.

## 13.2 Supplementary Figure 2.

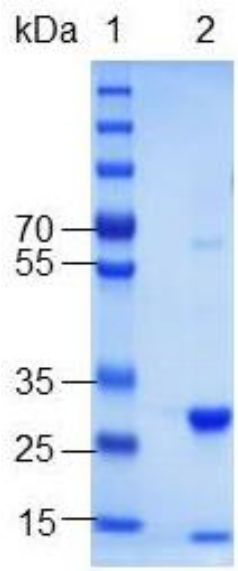


**Supplementary Figure 2. Production of recombinant Car4 enzyme.**

Gel electrophoretic analysis of recombinant Car4 enzyme. The recombinant protein was expressed in E. coli, purified with affinity column, dialyzed and separated on gradient SDS/PAGE gels, and detected with Coomassie Blue staining. The major band at 30 kDa represents full length recombinant Car4 and minor bands of 60 kDa and 15 kDa represent dimeric and proteolytically nicked Car4.

## 13.3 Supplementary Figure 3.

A

| | Control | CA IV | CA INH. |
|---|---|---|---|
| Day 0 | 29.1 ± 6.7 | 31.5 ± 6.2 | 32.3 ± 7.0 |
| Day 5 | 28.0 ± 7.4 | 32.4 ± 9.4 | 36.3 ± 6.8 |

B

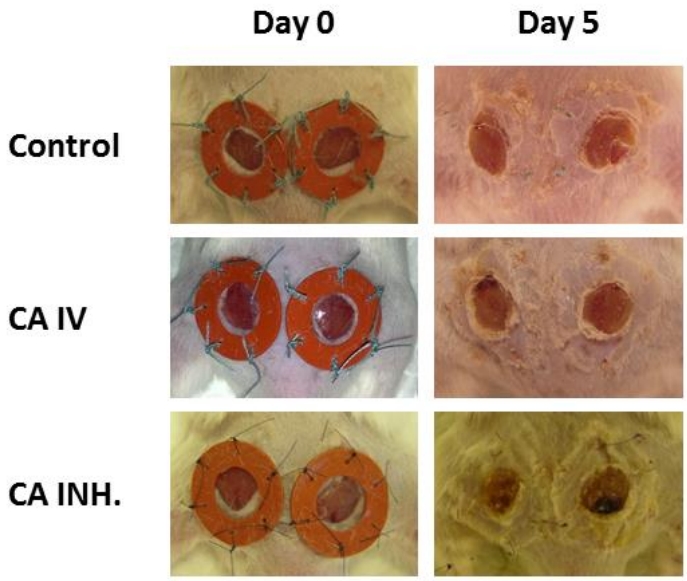


**Supplementary Figure 3. Wound closure in mice treated with recombinant Car4 enzyme.** Mice with full thickness skin excision wounds were treated with either recombinant Car4 enzyme or CA inhibitor applied on wound topically immediately after the wounding. Wounds were harvested on day 5, and the wound size (*A*) and closure were assessed from digital photos using ImageJ program and expressed as $mm^2$. (*B*) Representative digital pictures of the wounds treated with recombinant CA IV or CA inhibitor and collected on day 5 after wounding are shown for wound size and closure.

## 13.4 Supplementary Table 1. Primers used for qPCR.

All primer pairs have been designed to span exons to amplify only mRNA but not genomic DNA.

The primers don't bind to known SNP positions.

| gene | primer sequence (5´- 3´)<br>**F**orward/**R**everse | product size |
|---|---|---|
| CA I | F: TTGATGACAGTAGCAACC<br>R: CCAGTGAACTAAGTGAAG | 161 |
| CA II | F: CAAGCACAACGGACCAGA<br>R: ATGAGCAGAGGCTGTAGG | 122 |
| CA III | F: GCTCTGCTAAGACCATCC<br>R: ATTGGCGAAGTCGGTAGG | 160 |
| CA IV | F: CTCCTTCTTGCTCTGCTG<br>R: GACTGCTGATTCTCCTTA | 145 |
| CA Vb | F: AATGGCTTGGCTGTGATAGG<br>R: GGCGTAGTGAGAGACCCAGA | 104 |
| CA VI | F: AAGATTGACGAGTATGCC<br>R: TAGGTGTAATAGTGGTGG | 145 |
| CA VII | F: CAATGACAGTGATGACAGAA<br>R: TCCAGTGAACCAGATGTAG | 160 |
| CAIX | F: CTGAAGACAGGATGGAGAAG<br>R: GCAGAGTGCGGCAGAATG | 221 |
| CA XII | F: CCTATGTTGGTCCTGCTG<br>R: CGTTGTAACCTTGGAACTG | 143 |
| CA XIII | F: AATACGACTCCTCACTCC<br>R: TGCCGCAACCTGTAGTTC | 116 |
| CA XV | F: AGCACAGCCTGGATGAGA<br>R: CAGACACAATGGCAGAGA | 170 |

## 13.5 Supplementary Table 2. Results of mapping RNA-Seq to CA gene annotations

CA transcripts were identified whose intron/exon boundaries exactly match (=) RNA-Seq data for various tissues. Expression of those tissues are given in FPKM.

| Tissue | ref gene id | ref_id | class code | FPKM norm | FPKM | cov | len | ref match len |
|---|---|---|---|---|---|---|---|---|
| b-cells | CA14 | ENST00000582010 | = | 87122.9 | 91022.1 | 762.22 | 1176 | 1514 |
| b-cells | CA11 | ENST00000084798 | = | 3448.2 | 3653.094 | 55.304 | 1821 | 1844 |
| b-cells | CA13 | ENST00000321764 | = | 2277.11 | 2742.349 | 26.322 | 3501 | 3815 |
| b-cells | CA3 | ENST00000522207 | = | 251.976 | 159.8924 | 1.7738 | 451 | 645 |
| b-cells | CA2 | ENST00000285379 | = | 640.757 | 640.8174 | 9.9529 | 1494 | 1717 |
| b-cells | CA5B | ENST00000474624 | = | 1546.2 | 1198.678 | 16.976 | 540 | 565 |
| b-cells | CA5B | ENST00000478923 | = | 3958.35 | 2490.461 | 35.27 | 458 | 578 |
| monocytes-healthy | CA11 | ENST00000599267 | = | 1003.44 | 298.9805 | 3.8704 | 378 | 381 |
| monocytes-healthy | CA11 | ENST00000594088 | = | 3271.37 | 795.5951 | 10.299 | 324 | 275 |
| monocytes-healthy | CA13 | ENST00000321764 | = | 3883.35 | 2590.069 | 20.093 | 3662 | 3815 |
| monocytes-healthy | CA2 | ENST00000285379 | = | 2887.26 | 1599.104 | 22.549 | 1443 | 1717 |
| nk | CA11 | ENST00000084798 | = | 2528.87 | 1892.243 | 25.673 | 1777 | 1844 |
| nk | CA8 | ENST00000317995 | = | 354.884 | 273.4874 | 3.8527 | 3265 | 3812 |
| nk | CA3 | ENST00000285381 | = | 371.297 | 267.6843 | 3.8554 | 1660 | 1753 |
| nk | CA5B | ENST00000478923 | = | 9493.39 | 5117.402 | 66.587 | 589 | 578 |
| macrophage-m2 | CA12 | ENST00000344366 | = | 2151.21 | 9164.784 | 4.5811 | 3734 | 2744 |
| macrophage-m2 | CA11 | ENST00000084798 | = | 37616.3 | 168812 | 92.635 | 1575 | 1844 |
| macrophage-m2 | CA2 | ENST00000285379 | = | 65333.7 | 283239.7 | 154.21 | 1443 | 1717 |
| macrophage-m2 | CA5B | ENST00000454127 | = | 2380.91 | 12330.23 | 6.2201 | 5340 | 2205 |
| keratinocytes-undif | CA12 | ENST00000178638 | = | 4344.74 | 6230.474 | 139.9 | 4083 | 6413 |
| keratinocytes-undif | CA11 | ENST00000084798 | = | 626.232 | 859.8755 | 20.392 | 1780 | 1844 |
| keratinocytes-undif | CA2 | ENST00000285379 | = | 1468.46 | 1948.369 | 50.135 | 1476 | 1717 |
| skin | CA6 | ENST00000377443 | = | 524.686 | 1888.604 | 16.219 | 1233 | 1319 |
| skin | CA14 | ENST00000369111 | = | 789.664 | 3458.73 | 30.645 | 2276 | 2403 |
| skin | CA12 | ENST00000344366 | = | 12078.4 | 37267.41 | 336.3 | 4032 | 2744 |
| skin | CA12 | ENST00000178638 | = | 26995.9 | 140397.4 | 1266.9 | 4065 | 6413 |
| skin | CA4 | ENST00000300900 | = | 107.319 | 359.4333 | 3.2884 | 860 | 1154 |
| skin | CA11 | ENST00000084798 | = | 2600.57 | 10466.45 | 88.309 | 1710 | 1844 |
| skin | CA8 | ENST00000317995 | = | 110.369 | 495.9338 | 4.4609 | 3532 | 3812 |
| skin | CA13 | ENST00000321764 | = | 1111.41 | 5058.904 | 45.134 | 3542 | 3815 |
| skin | CA1 | ENST00000523022 | = | 182.5 | 644.5951 | 4.7867 | 1055 | 1208 |
| skin | CA3 | ENST00000285381 | = | 940.788 | 4074.264 | 35.885 | 1745 | 1753 |
| skin | CA2 | ENST00000285379 | = | 17679.2 | 73994.29 | 688.66 | 1561 | 1717 |
| skin | CA9 | ENST00000378357 | = | 2254.86 | 8751.696 | 79.151 | 1507 | 1618 |
| macrophage-m1 | CA12 | ENST00000344366 | = | 23522.3 | 59399.86 | 79.78 | 3742 | 2744 |
| macrophage-m1 | CA12 | ENST00000178638 | = | 27296.2 | 65408.2 | 87.849 | 3775 | 6413 |

| | | | | | | | | |
|---|---|---|---|---|---|---|---|---|
| macrophage-m1 | CA11 | ENST00000084798 | = | 17346.9 | 39907.33 | 54.74 | 1730 | 1844 |
| macrophage-m1 | CA2 | ENST00000285379 | = | 119454 | 264718.7 | 375.86 | 1433 | 1717 |
| macrophage-m1 | CA5B | ENST00000498004 | = | 3350.94 | 6219.821 | 8.2757 | 717 | 488 |
| neutrophils | CA4 | ENST00000300900 | = | 19051 | 14791.68 | 173.57 | 1152 | 1154 |
| neutrophils | CA2 | ENST00000285379 | = | 996.678 | 765.6827 | 9.7061 | 1463 | 1717 |
| cd4 | CA11 | ENST00000084798 | = | 2824.52 | 3659.525 | 46.077 | 1759 | 1844 |
| cd4 | CA5B | ENST00000478923 | = | 7897.18 | 7214.55 | 83.642 | 550 | 578 |
| dermal-fibroblasts | CA12 | ENST00000344366 | = | 132367 | 70010.04 | 933.04 | 6372 | 2744 |
| dermal-fibroblasts | CA11 | ENST00000084798 | = | 3075.12 | 1513.818 | 20.175 | 1829 | 1844 |
| dermal-fibroblasts | CA13 | ENST00000321764 | = | 2867.36 | 1585.355 | 21.128 | 3771 | 3815 |
| dermal-fibroblasts | CA9 | ENST00000378357 | = | 81208.8 | 38762.42 | 516.59 | 1618 | 1618 |
| keratinocytes-dif | CA14 | ENST00000582010 | = | 50512.5 | 78051.22 | 890.39 | 1445 | 1514 |
| keratinocytes-dif | CA12 | ENST00000178638 | = | 6963.37 | 9150.187 | 169.69 | 4126 | 6413 |
| keratinocytes-dif | CA11 | ENST00000084798 | = | 727.176 | 952.2422 | 18.887 | 1835 | 1844 |
| keratinocytes-dif | CA2 | ENST00000285379 | = | 2115.47 | 2529.393 | 52.97 | 1468 | 1717 |
| cd8 | CA14 | ENST00000582010 | = | 115928 | 93747.34 | 656.77 | 1165 | 1514 |
| cd8 | CA11 | ENST00000084798 | = | 3791.96 | 3127.982 | 39.633 | 1799 | 1844 |
| cd8 | CA2 | ENST00000285379 | = | 651.919 | 493.62 | 6.5076 | 1307 | 1717 |
| cd8 | CA5B | ENST00000318636 | = | 63903 | 57353.93 | 415.43 | 6775 | 6835 |

## 13.6 Supplementary Table 3. Gene ontology enrichment analysis of 1063 genes with a correlation of expression with CA4 of 0.5 or greater in skin.

Correlation of expression data was retrieved from the Medisapiens database of microarray experiments, and GO enrichment analysis was performed using

| GO biological process | ref | actual | expected | fold change | P-value |
|---|---|---|---|---|---|
| regulation of natural killer cell chemotaxis (GO:2000501) | 8 | 6 | 0.38 | 15.79 | 2.27E-002 |
| neutrophil chemotaxis (GO:0030593) | 64 | 16 | 3.03 | 5.28 | 1.01E-003 |
| granulocyte chemotaxis (GO:0071621) | 68 | 17 | 3.22 | 5.28 | 4.13E-004 |
| neutrophil migration (GO:1990266) | 67 | 16 | 3.17 | 5.05 | 1.84E-003 |
| granulocyte migration (GO:0097530) | 72 | 17 | 3.41 | 4.99 | 9.17E-004 |
| cellular defense response (GO:0006968) | 61 | 14 | 2.89 | 4.84 | 1.62E-002 |
| positive regulation of leukocyte chemotaxis (GO:0002690) | 78 | 17 | 3.69 | 4.61 | 2.75E-003 |
| myeloid leukocyte migration (GO:0097529) | 95 | 20 | 4.5 | 4.44 | 4.58E-004 |
| leukocyte chemotaxis (GO:0030595) | 115 | 24 | 5.44 | 4.41 | 2.66E-005 |
| regulation of leukocyte chemotaxis (GO:0002688) | 92 | 19 | 4.35 | 4.37 | 1.30E-003 |
| chemokine-mediated signaling pathway (GO:0070098) | 73 | 15 | 3.45 | 4.35 | 2.67E-002 |
| positive regulation of chemotaxis (GO:0050921) | 114 | 22 | 5.39 | 4.08 | 4.53E-004 |
| positive regulation of behavior (GO:0048520) | 135 | 25 | 6.39 | 3.91 | 1.28E-004 |
| positive regulation of leukocyte migration (GO:0002687) | 103 | 19 | 4.87 | 3.90 | 6.86E-003 |
| regulation of chemotaxis (GO:0050920) | 152 | 27 | 7.19 | 3.76 | 8.12E-005 |
| cell chemotaxis (GO:0060326) | 164 | 28 | 7.76 | 3.61 | 9.97E-005 |
| regulation of behavior (GO:0050795) | 208 | 34 | 9.84 | 3.46 | 8.45E-006 |
| cellular response to interferon-gamma (GO:0071346) | 127 | 20 | 6.01 | 3.33 | 3.75E-002 |
| regulation of leukocyte migration (GO:0002685) | 139 | 21 | 6.58 | 3.19 | 4.10E-002 |
| leukocyte migration (GO:0050900) | 256 | 38 | 12.11 | 3.14 | 1.23E-005 |
| regulation of vasculature development (GO:1901342) | 211 | 29 | 9.99 | 2.90 | 4.82E-003 |
| regulation of angiogenesis (GO:0045765) | 195 | 26 | 9.23 | 2.82 | 3.07E-002 |
| regulation of endocytosis (GO:0030100) | 195 | 26 | 9.23 | 2.82 | 3.07E-002 |
| inflammatory response (GO:0006954) | 432 | 55 | 20.44 | 2.69 | 8.24E-007 |
| regulation of peptide transport (GO:0090087) | 264 | 33 | 12.49 | 2.64 | 6.60E-003 |
| cellular calcium ion homeostasis (GO:0006874) | 284 | 34 | 13.44 | 2.53 | 1.15E-002 |
| calcium ion homeostasis (GO:0055074) | 298 | 35 | 14.1 | 2.48 | 1.24E-002 |
| cellular divalent inorganic cation homeostasis (GO:0072503) | 298 | 35 | 14.1 | 2.48 | 1.24E-002 |
| divalent inorganic cation homeostasis (GO:0072507) | 320 | 37 | 15.14 | 2.44 | 9.00E-003 |
| regulation of response to wounding (GO:1903034) | 383 | 43 | 18.13 | 2.37 | 2.70E-003 |
| positive regulation of response to external stimulus (GO:0032103) | 383 | 43 | 18.13 | 2.37 | 2.70E-003 |
| ion homeostasis (GO:0050801) | 559 | 62 | 26.45 | 2.34 | 1.11E-005 |
| metal ion homeostasis (GO:0055065) | 470 | 51 | 22.24 | 2.29 | 6.29E-004 |
| cellular metal ion homeostasis (GO:0006875) | 398 | 42 | 18.83 | 2.23 | 1.72E-002 |
| synaptic transmission (GO:0007268) | 560 | 59 | 26.5 | 2.23 | 1.66E-004 |
| inorganic ion homeostasis (GO:0098771) | 533 | 56 | 25.22 | 2.22 | 4.17E-004 |
| cation homeostasis (GO:0055080) | 519 | 54 | 24.56 | 2.20 | 9.78E-004 |
| cellular cation homeostasis (GO:0030003) | 435 | 45 | 20.59 | 2.19 | 1.26E-002 |
| cellular ion homeostasis (GO:0006873) | 445 | 46 | 21.06 | 2.18 | 9.90E-003 |
| cellular chemical homeostasis (GO:0055082) | 526 | 51 | 24.89 | 2.05 | 1.63E-002 |

# 14. SUPPLEMENTARY METHODS

## 14.1 Extraction of RNA

Skin wound samples and retinas were collected, snap frozen in liquid nitrogen, stored at −80 °C, and preserved in Ambion RNALater ICE Frozen Tissue Transition Solution (Life Technologies). The mRNA was then extracted using Invitrogen Trizol Reagent (Life Technologies) as described previously, with bead homogenization performed via Precellys' 2 ml tubes and Precellys®24 (Bertin Technologies, Villeurbanne, France) homogenizer at 4 °C (May et al., 2015). After the addition of chloroform and centrifugation, the aqueous phase was transferred to RNeasy columns (Qiagen, Hilden, Germany) and mRNA purification continued according to the manufacturer's instructions. The concentration and quality of RNA was determined by Nanodrop A260 measurement (May et al., 2015).

## 14.2 Immunohistochemistry (IHC)

Hematoxylin/eosin (HE) and IHC stainings were performed on 6 μm thick paraffin sections. The following primary antibodies were used for IHC: rabbit anti-mouse CA IV (1:100) and rabbit anti-mouse CA IX (1:300) (Brion et al., 1997; Gut et al., 2002). For the control stainings, the primary anti-CA sera were replaced with normal rabbit serum (NRS). The immunostaining was performed as described previously in detail using the Vectastain Elite ABC Reagent kit (Vector Laboratories) with 3,3'-Diaminobenzidine tetrahydrochloride (DAB) Substrate Kit (Invitrogen). Finally, the sections were examined and photographed with a Zeiss Axioskop 40 microscope (Carl Zeiss, Göttingen, Germany).

## 14.3 Histology

Wound tissue was harvested at five days (n=5 per group) after wounding. Mice were euthanized and perfused by intra-cardial injection of 4 % paraformaldehyde (PFA). Excision of a rectangular section of skin containing all wounds, as well as underlying skeletal muscle, was performed to ensure the uninterrupted wound architecture. The "whole-mounted" sections were immobilized on filter paper, immersed in 4% PFA for additional O/N fixation, and washed with physiological saline. After O/N fixation, the wounds were bisected, dehydrated, and embedded in paraffin. Longitudinal sections (6 μm) from the middle of the wound were stained with HE.

## 14.4 Morphological assessment of wound closure

After the surgery and during the sacrifice, the wound were photographed digitally. Two 2 x 2 cm cardboard squares were placed on both sides of the animal to adjust the digital pictures taken from various distance in relation to wounds and the total area of wound was measured and analyzed from digital photographs using ImageJ software by manually drawing the edges of each individual wound.

## 14.5 Quantitative analysis of histology

Two HE-stained sections from the middle of each wound were quantitatively evaluated, and the average of the two values was used in the analysis. The length of epithelial tongues (a measure of re-epithelialization) was measured as described by Chen et al. (Chen et al., 2015) and the size of granulation tissue was determined. Image analysis and quantification of histological parameters, were performed using Spectrum digital pathology system (Aperio Technologies) using the Aperio

ScanScope CS and XT systems (Aperio Technologies) as described previously elsewhere (Järvinen and Ruoslahti, 2010). Slides were viewed and analyzed with the ImageScope viewer. The areas of interests were recorded manually for each wound.

## 14.6 Oxygen-induced retinopathy (OIR) model

The experiments utilizing the OIR model were carried out as described in detail previously (Smith et al., 1994; Uusitalo-Jarvinen et al., 2007). Briefly, neonatal C57BL/6 mice at P7 and their nursing mother were exposed to 75% oxygen for 5 days in a custom-made oxygen chamber (Smith et al., 1994; Uusitalo-Jarvinen et al., 2007). At P12, the mice were returned to normal room air. As postnatal weight gain has been shown to affect outcome in the OIR model, the pups were weight-matched (Stahl et al., 2010). All OIR experiments were performed according to the ARVO statement for the use of animals in ophthalmic and vision research.

## 14.7 Promoter analysis of the primary CA4 transcript

A computational comparative genomics analysis was performed on the promoter region of the human *CA4* gene (Ensembl: ENSG00000167434), defined as the region 900 base pairs (bp) upstream and 100 bp downsteam of the transcription start site (TSS). Of the four protein coding transcripts for this gene identified in the Ensembl database, human transcript ENST00000300900 (CA4-001) was chosen based on our analysis of RNA-Seq data. This transcript encodes a full-length 312 amino acid (aa) protein while the others produce significantly shorter (38-184 aa) polypeptides. An alignment of the corresponding promoter nucleotide sequences of 15 mammalian species (including human) was retrieved from the Ensembl database. Experimentally determined binding sites for transcription factors were retrieved from the Jaspar database from which dinucleotide weight matrices were

produced for log likelihood scoring of potential transcription factor binding sites (TFBSs). After scoring all possible positions in the nucleotide sequences of all species, locations where high scoring potential TFBSs were observed in multiple species were identified.

## 14.8 GO analysis of proteins

The Medisapiens database (Kilpinen et al., 2008) (http://ist.medisapiens.com/) houses data from a large number of microarray expression studies. For skin tissue there were at least 135 microarray experiment samples for all genes present on a human genome U133 chip. We extracted all expression correlation values for CA4 with all other genes. The subset of these genes that had a positive correlation of expression of 0.50 or greater totaled 1,063, which were then used to perform a biological processes gene ontology enrichment analysis using the (http://geneontology.org) webserver (Ashburner et al., 2000; Gene Ontology Consortium, 2015). The gene ontology terms which were enriched among our subset of CA4 positively correlated genes at 2-fold or greater were then analyzed for biological significance.

# 15. REFERENCES FOR SUPPLEMENTARY METHODS

(1) May U, Prince S, Vähätupa M, Laitinen AM, Nieminen K, Uusitalo-Järvinen H, et al. Resistance of R-Ras knockout mice to skin tumour induction. Sci Rep 2015 Jul 2;5:11663.

(2) Brion LP, Cammer W, Satlin LM, Suarez C, Zavilowitz BJ, Schuster VL. Expression of carbonic anhydrase IV in carbonic anhydrase II-deficient mice. Am J Physiol 1997 Aug;273(2 Pt 2):F234-45.

(3) Gut MO, Parkkila S, Vernerova Z, Rohde E, Zavada J, Hocker M, et al. Gastric hyperplasia in mice with targeted disruption of the carbonic anhydrase gene Car9. Gastroenterology 2002 Dec;123(6):1889-1903.

(4) Chen L, Mirza R, Kwon Y, DiPietro LA, Koh TJ. The murine excisional wound model: Contraction revisited. Wound Repair Regen 2015 Nov 12;23(6):874-877.

(5) Järvinen TA, Ruoslahti E. Target-seeking antifibrotic compound enhances wound healing and suppresses scar formation in mice. Proc Natl Acad Sci U S A 2010 Dec 14;107(50):21671-21676.

(6) Smith LE, Wesolowski E, McLellan A, Kostyk SK, D'Amato R, Sullivan R, et al. Oxygen-induced retinopathy in the mouse. Invest Ophthalmol Vis Sci 1994 Jan;35(1):101-111.

(7) Uusitalo-Jarvinen H, Kurokawa T, Mueller BM, Andrade-Gordon P, Friedlander M, Ruf W. Role of protease activated receptor 1 and 2 signaling in hypoxia-induced angiogenesis. Arterioscler Thromb Vasc Biol 2007 Jun;27(6):1456-1462.

(8) Stahl A, Chen J, Sapieha P, Seaward MR, Krah NM, Dennison RJ, et al. Postnatal weight gain modifies severity and functional outcome of oxygen-induced proliferative retinopathy. Am J Pathol 2010 Dec;177(6):2715-2723.

(9) Kilpinen S, Autio R, Ojala K, Iljin K, Bucher E, Sara H, et al. Systematic bioinformatic analysis of expression levels of 17,330 human genes across 9,783 samples from 175 types of healthy and pathological tissues. Genome Biol 2008;9(9):R139-2008-9-9-r139. Epub 2008 Sep 19.

(10) Gene Ontology Consortium. Gene Ontology Consortium: going forward. Nucleic Acids Res 2015 Jan;43(Database issue):D1049-56.

(11) Ashburner M, Ball CA, Blake JA, Botstein D, Butler H, Cherry JM, et al. Gene ontology: tool for the unification of biology. The Gene Ontology Consortium. Nat Genet 2000 May;25(1):25-29.